Available online at www.sciencedirect.com
ScienceDirect
Polymer 48 (2007) 7078–7086
polymer
www.elsevier.com/locate/polymer

Synthesis and characterization of methacrylate phospho-silicate hybrid for thin film applications

Aravindaraj G. Kannan, Namita Roy Choudhury*, Naba K. Dutta

ARC Special Research Centre for Particle and Material Interfaces, Ian Wark Research Institute, University of South Australia, Mawson Lakes, South Australia 5095, Australia

Received 16 August 2007; received in revised form 25 September 2007; accepted 28 September 2007
Available online 6 October 2007

Abstract

Phosphorus containing methacrylate hybrids were synthesized from 2-(methacryloyloxy)ethyl phosphate (EGMP) and 3-[(methacryloyloxy)-propyl] trimethoxysilane (MEMO) via dual-cure process involving sol–gel reaction and addition polymerization. The kinetics of the reactions was established using spectroscopic techniques. Photoacoustic Fourier transform infrared spectroscopy (PA-FTIR) and X-ray photoelectron spectroscopy (XPS) confirm the formation of Si–O–Si, P–O–P and Si–O–P linkages and simultaneous polymerization of methacrylate groups leading to a dense networked structure. The presence of silicate/phospho-silicate network in the hybrid enhances its thermal stability. Nano-indentation measurements on thin films show enhanced hardness and modulus with increasing silicate network. Topographic and conductivity images obtained using micro-thermal analysis (μTA) reveal a dense, homogenous and defect-free thin film formed on metallic substrate with a T_g of 93 °C.

Keywords: Hybrid thin film; Phospho-silicate; Interpenetrating network

1. Introduction

In recent years, phosphorus containing polymers have gained significant interest due to their unique characteristics in different applications such as reduced flammability, increased adhesion to metals, corrosion protection, membranes, biomedical areas etc. Phosphorus containing compounds when remain as additives in a physical mixture, can be depleted by evaporation or leaching by solvent or water. Such disadvantage can be overcome if they form a part of polymer network structure [1]. To achieve this goal, several approaches [2–4] of controlled homo or copolymerization have been investigated using phosphate precursors. However, phosphorus containing monomers can also be hybridized with other inorganic and organic precursor to form a new class of hybrid, which offers beneficial synergism between the properties of organic and inorganic materials. The ability to tailor the properties of such hybrids, at a molecular level, signifies their enormous potential in a wide variety of technologically advanced and conventional application fields [5–7].

There are several routes to form hybrid materials [8] on a nanoscale, but the most commonly employed method is the sol–gel method [9,10], a simple process that allows the synthesis of hybrid at a relatively lower temperature at which organic compounds are stable. This can be achieved either through the sol–gel process in presence of a preformed polymer or polymerization in sol–gel networks or simultaneous formation of interpenetrating networks or using dual-network precursors. Among these types, the dual-network precursor method leads to strong covalent bonding between organic and inorganic components. Since the strength of interaction in this hybrid is much higher than the hybrid formed through other methods, it allows a better degree of homogeneity, transparency, thermal resistance and mechanical properties in the final hybrid [11,12]. Hence, this class of hybrid with strong interaction is most commonly used for thin film applications.

* Corresponding author. Tel.: +61 8 8302 3719; fax: +61 8 8302 3755.
E-mail address: namita.choudhury@unisa.edu.au (N.R. Choudhury).

0032-3861/$ - see front matter © 2007 Elsevier Ltd. All rights reserved.
doi:10.1016/j.polymer.2007.09.050

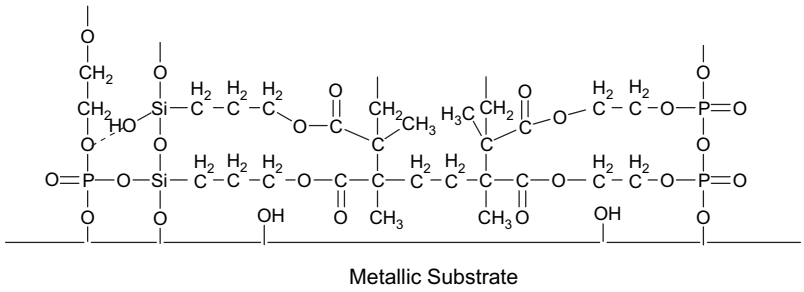

Scheme 1. Proposed structure of the hybrid network coated on metallic substrate.

[3-(Methacryloyloxy)propyl]trimethoxysilane (MEMO) is one of the most important precursors with dual-network forming capability. It has a polymerizable methacryloxy group at one end and the alkoxy silane groups capable of forming inorganic networks via sol–gel route at the other end. These hybrid materials can form a transparent, dense, uniform thin film on various substrates. It can combine the flexibility, density, toughness and easy processability of the organic component with the hardness, chemical and weather resistance of the inorganic component, thereby exhibiting multifunctional behavior. MEMO has been either homo or copolymerized with methyl methacrylate or acrylonitrile resulting in a uniformly distributed, transparent hybrid material [13,14]. MEMO has also been used as a coupling agent to compatibilize organic and inorganic phases [15]. Till now, no attempt has been made to utilize the beneficial properties of phosphorus containing precursors with MEMO for thin film applications.

In this work, we have chosen to copolymerize 2-(methacryloyloxy)ethyl phosphate (EGMP) containing a polymerizable methacrylate group and functional phosphate group with MEMO. The selected materials thus have unique combination of three different components namely methacryloxy, phosphate functionality and silicon–alkoxy groups. The hydrolysable silicon alkoxide at one end can be condensed to form inorganic Si–O–Si, Si–O–P networks and simultaneous polymerization of the methacrylate group at the other end can lead to highly cross-linked dense networked structure [13]. Also, incorporation of the phosphate can improve thin film adhesion through acid–base type interaction of dissociated $P–O^-$ from EGMP with M^{n+} of the metallic substrate rather than forming P=O/metal bond through induced dipole [16,17]. The possible structure of the proposed hybrid network on a metallic substrate is given in Scheme 1.

2. Experimental section

2.1. Materials

MEMO, EGMP, acetone and hexane were purchased from Aldrich, Australia and used without further purification. Ethanol was used as a solvent. Commercial alkaline cleaner was purchased for the final cleaning of mild steel substrates.

2.2. Synthesis of methacrylate phospho-silicate hybrid

The hybrid material was synthesized in a two-step reaction process. Since a pre-hydrolysis of the sol–gel reactants promotes molecular scale mixing [18], 5 mmol of MEMO was first hydrolyzed in 10 mmol/15 mmol of ethanol/water solution mixture at room temperature. The progress of the hydrolysis reaction was monitored via transmission FTIR and the reaction was deemed complete when the methoxy group peak at 2841 cm^{-1} disappeared completely. The reaction was complete in 6 h. The resulting hydrolyzed solution was mixed with 5 mmol of EGMP and stirred vigorously at 65 °C for 1 h before thin film coating. Attempts have been made with peroxide initiator (0.1 and 0.01 wt%); but the reaction rates are found to be very fast. The viscosity of the sol, an important parameter during thin film formation, was difficult to control. Hence, the reactions were continued with thermal polymerization. For bulk analysis such as TGA and DSC, 1.5 g of the resulting sol was transferred to a petri dish and was thermally cured at 80 °C to prepare the hybrid material (henceforth referred as MEMO/EGMP – 1:1).

The remaining sol was diluted with ethanol to 20% and vigorously stirred for 5 min for complete dissolution. The hybrid thin film was applied on steel substrates via the following procedure: The mild steel substrates were sequentially polished using abrasive papers with grit numbers 800, 1000 and 1200 prior to cleaning by sequential immersion for 10 min each in acetone, hexane and ethanol solutions to remove surface oils. The substrates were rinsed with distilled water and dried between each solvent wash and after the final solvent wash. Finally, the dried substrate was treated with a commercial alkaline cleaner and rinsed with distilled water and dried. The purpose of the alkaline cleaner treatment was to produce a fresh layer of oxide on the substrate surface for chemical bonding to the phosphate group. The cleaned mild steel substrate was then dip-coated into the diluted sol for 4 min and the coated sample was dried at room temperature for 24 h to allow solvent evaporation. The thin film was thermally cured at 120 °C for 2 h in an oven, when further condensation/polymerization reaction took place at the substrate interface to form a hybrid network. Similar experimental procedures were used to synthesize hybrids at other compositions namely MEMO/EGMP – 7:3 and MEMO/EGMP – 3:7.

2.3. Spectroscopic characterization

The spectroscopic characterization of the monomers and the progress of hydrolysis reaction were monitored using transmission mode FTIR. Sodium chloride plates were used as window material. The curing reaction of the hybrid was monitored using photoacoustic Fourier transform infrared spectroscopy (PA-FTIR) [19]. A Nicolet Magna™ IR spectrometer (model 750) equipped with a MTEC (model 300) photoacoustic cell was used. The spectra were collected in the mid-infrared region with 156 scans at a resolution of 4 cm^{-1} and a mirror velocity of 0.158 cm/s. Carbon black was used as a reference and the system was purged with helium gas at a flow rate of 10–20 cm^3/s.

X-ray photoelectron spectroscopy (XPS) was carried out using Kratos Axis Ultra Spectrometer, equipped with an Al-Kα X-ray source ($h\nu = 1486.7$ eV). The coated mild steel (MEMO/EGMP – 1:1 ratio) samples were characterized at a photoelectron take-off angle of 90° to the sample surface. The charge correction was performed by fixing the hydrocarbon component of the C 1s peak to 284.7 eV.

2.4. Thermal analysis

Thermal stability of the prepared hybrids was investigated using thermogravimetric analyzer (TGA), TA instruments (model 2950), at a heating rate of 10 °C/min from room temperature to 900 °C under a controlled gas flow rate of 50 mL/min. The sample was heated from room temperature to 550 °C in nitrogen and between 550 and 900 °C in oxygen. The mass of the sample used was between 10 and 12 mg. The onset of degradation, weight loss due to different components and remaining residue were evaluated. The temperature of the maximum weight loss was determined from differential thermogravimetric (DTG) curves.

Differential scanning calorimetry (DSC) was performed using a TA instrument DSC (model 2920) with a heating and cooling rate of 10 °C/min under nitrogen atmosphere. The mass of the sample taken was between 8 and 10 mg and the sample was cycled twice through a temperature range of 25–200 °C.

2.5. Micro-thermal analysis (μTA)

Scanning thermal microscopy was carried out using μTA, TA instruments (model 2990), with a thermal probe. It can scan the surface using an AFM tip and collect images related to the topography and thermal conductivity of the surface [20]. The topographic and conductivity imaging of the coated mild steel sample was done with the thermal probe heated at 50 °C. Also, local thermal analysis (LTA) was carried out using μTA, where the thermal probe tip temperature was ramped from room temperature to 500 °C at a rate of 10 °C/s. LTA allows random positioning of the probe on the coated mild steel sample and monitoring the vertical motion of the probe during heating thereby studying its thermomechanical properties.

2.6. Mechanical properties of the hybrid

The mechanical properties of the hybrid thin film on mild steel substrate were evaluated using ultra-micro indentation system (UMIS 2000, CSIRO Australia) with a Berkovich indenter. The calibration of the indentation system was carried out with fused silica (elastic modulus $E = 72$ GPa) at 0.2 mN peak load. The indentations were carried out after allowing enough time for the samples to attain thermal equilibrium (drift rate < 1 nm/min) in the indentation chamber. Thermal drift during the experiment was deemed negligible and no thermal corrections were made during analysis. The nanoindentation load–displacement experiments were done with step loading to the maximum load, hold period at the maximum load of 30 s and the unloading. A series of 20 indentations were made with the gap of 50 μm spacing. The average elastic modulus and hardness values were determined from the load–displacement data after making necessary corrections for area factor and initial penetration depth.

3. Results and discussion

3.1. Structural evolution of the hybrid

PA-FTIR was used to evaluate the final structure of the hybrid. The FTIR spectra of MEMO, EGMP and the hybrid material (1:1 ratio) are shown in Fig. 1. The bands at 1635 cm^{-1}, 1405 cm^{-1} and 817 cm^{-1}, that are present in the unreacted MEMO and EGMP monomers correspond to C=C, $=CH_2$ wag, $=CH_2$ twist, respectively [13,21,22]. These bands are weak and present in the cured hybrid indicating the reduction of the double bond (C=C) in two monomers and subsequent network formation through the addition polymerization. As a result, the peak at 1719 cm^{-1} corresponding to C=O conjugated with C=C [13,21] becomes non-conjugated and shifts to higher wavenumber at 1735 cm^{-1}. The peaks in the region of 1300 cm^{-1}–950 cm^{-1} merge and form a very broad peak. Usually, the peaks corresponding to inorganic materials appear in this region. Therefore, in order to understand the interaction

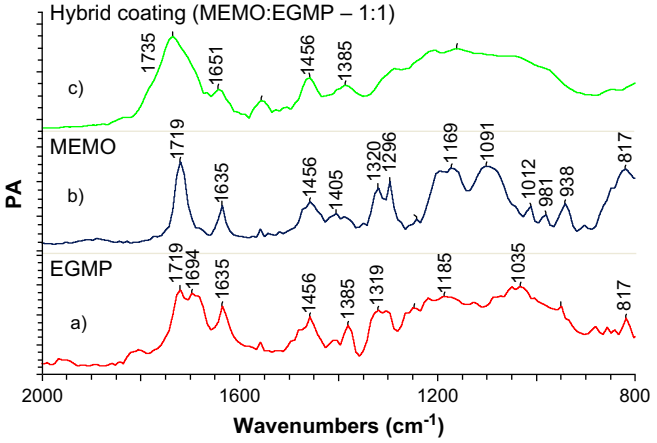

Fig. 1. FTIR spectra of (a) EGMP; (b) MEMO and (c) hybrid thin film prepared at 1:1 ratio in arbitrary scales.

of the inorganic components, the broad peak was deconvoluted by Gaussian deconvolution method using PeakFit 4 software program and the deconvoluted spectrum is shown in Fig. 2. The band at 1091 cm^{-1} corresponding to Si–O–C bond [13] in MEMO disappears completely and a new broad band appears at 1108 cm^{-1} which is assigned to Si–O–Si network. This shows that the methoxy group attached to silicon in the MEMO is completely hydrolyzed and condensed to form Si–O–Si network [13,23]. Also, the P–OH groups in the EGMP condense to form the P–O–P and P–O–Si linkages [24] which are confirmed by the appearance of peaks at 945 cm^{-1} and 1160 cm^{-1}. The peaks corresponding to the P–O–C band at 981 cm^{-1} and 1037 cm^{-1} and the Si–CH_2 peak at 1209 cm^{-1} remain unchanged. Also, the ester peaks present in this region remain unchanged. Similar observation has been made with 3:7 and 7:3 MEMO/EGMP materials. These results show that MEMO and EGMP react to form a highly cross-linked hybrid through the formation of Si–O–Si, P–O–P and P–O–Si inorganic networks and an organic network through the polymerization of methacrylate group.

FTIR was also used to understand the dual-cure reactions occurring during the first stage and the subsequent thermal curing stage of the thin film. During the first stage hydrolysis of MEMO (spectra not shown), the peak at 2841 cm^{-1}, which corresponds to the methoxy group (–OCH_3) [25] in MEMO, disappears completely, whereas a new broad peak appears at 3400 cm^{-1}. The appearance of the new peak shows the formation of the silanol groups, which lead to hydrogen bonding with the carboxyl groups and is confirmed by the appearance of a shoulder peak at 1696 cm^{-1}. The second stage condensation/polymerization reaction during the thermal curing of the thin film (MEMO/EGMP – 1:1 ratio) at 120 °C was monitored via PA-FTIR and the spectra of the as-prepared thin film, after 30 min, 60 min, 90 min and 120 min of curing are given in Fig. 3. All the peaks corresponding to the methacryloxy group in MEMO and EGMP are present in the spectra. As discussed earlier, the peaks at 1635 cm^{-1}, 1405 cm^{-1}, and 817 cm^{-1} decrease progressively with the curing time. The degree of addition polymerization (DP) at various times during the curing stage of the hybrid was calculated from the area of the peak at 1635 cm^{-1} using the following formula:

$$DP_x = [1 - (A_x/A_0)]100 \quad (1)$$

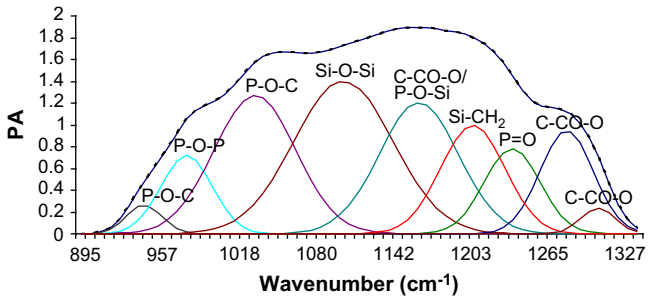

Fig. 2. Deconvoluted IR spectra in the region of 895 cm^{-1}–1327 cm^{-1}.

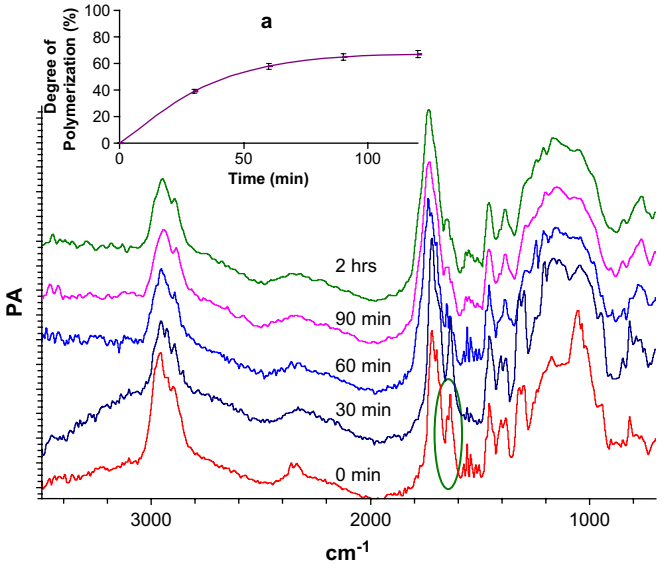

Fig. 3. FTIR spectra of the hybrid thin film (1:1 ratio) at different curing times in arbitrary photoacoustic scales; (a) degree of polymerization at different curing times.

where DP_x is the DP at "x" time ($x = 30$, 60, 90 and 120 min) and A_0 and A_x are the areas of the peak (at 1635 cm^{-1}) at 0 min and x min, respectively. The plot of degree of polymerization with time is given in Fig. 3(a). Like other polymerization reactions, initial rate of polymerization is faster and reaches a plateau at around 70% conversion. From the slope of the curve, the conversion rate was determined as 1.30, 0.63, 0.23 and 0.07%/min at 10, 39, 58 and 65% degree of polymerization, respectively. The plateau at 70% conversion indicates that the reaction is incomplete and this may be due to the hybrid formation through simultaneous inorganic polycondensation reactions and addition polymerization. As the molecular weight and the crosslinking density increase, the mobility of the molecules is reduced, thereby reducing the probability of further reaction due to gel effect. Also, the peak at 1696 cm^{-1} corresponding to hydrogen bonded C=O, conjugated with C=C disappears progressively and the peak at 1719 cm^{-1} shifts to 1735 cm^{-1} indicating the disappearance of the double bond. At the same time, the peaks between 1300 cm^{-1} and 950 cm^{-1} merge and form a broad peak, as discussed earlier indicating the interaction of the inorganic components. Also, a new peak appears at 1656 cm^{-1}, which corresponds to H–O–H deformation. This indicates the formation of water, as a result of condensation reactions.

Further evaluation of the structure of the hybrid (1:1 ratio) coated on mild steel substrate was carried out using XPS. As expected, the survey spectrum shows the presence of silicon, phosphorus, carbon and oxygen. To further investigate the structure of the coated hybrid, multiplexed spectra for Si 2p, P 2p, C 1s and O 1s are obtained and shown in Fig. 4(a)–(d), respectively. The C 1s peak is broad and deconvoluted into four peaks centered at 284, 284.7, 286.4 and 288.6 eV, respectively. The peaks at 284 eV and 284.7 eV correspond to the carbon bonded to silicon atom (C–Si) and

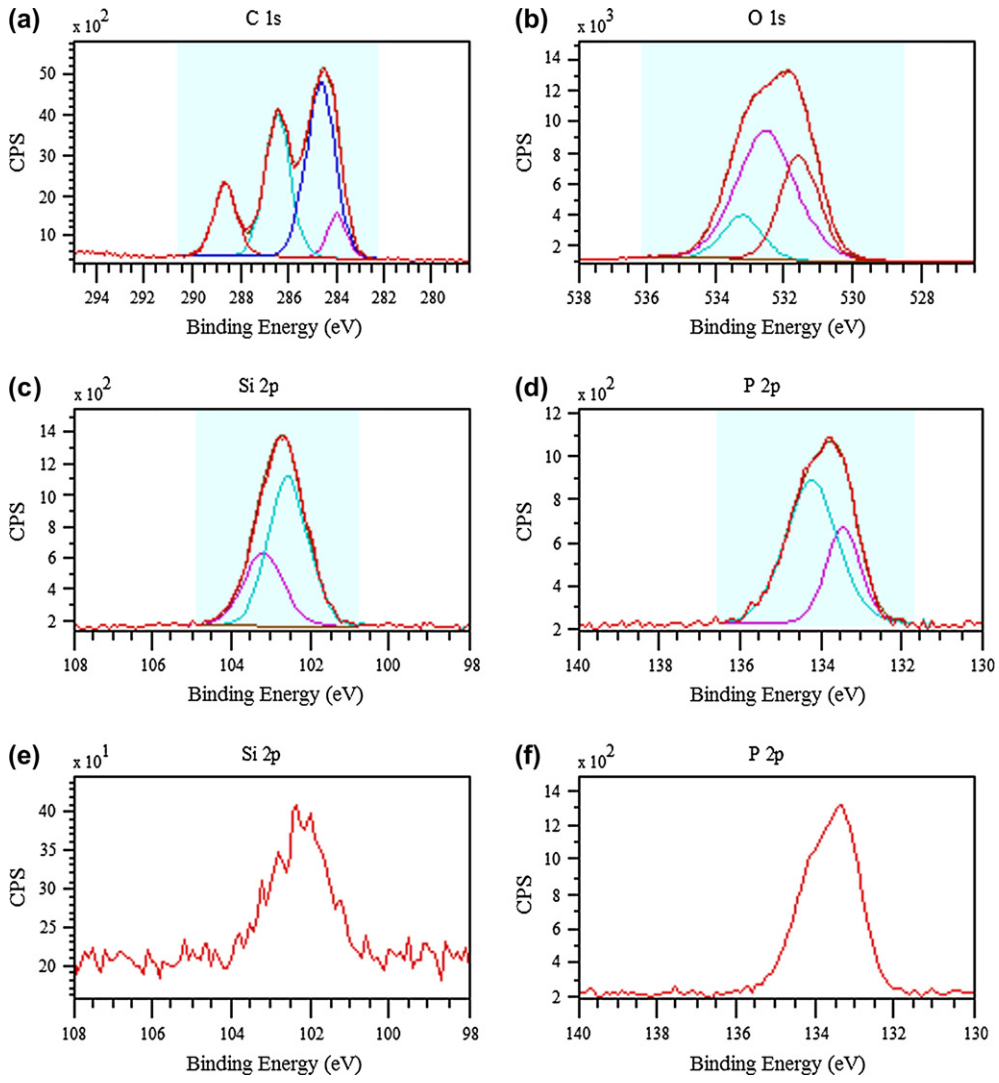

Fig. 4. (a) C 1s; (b) O 1s; (c) Si 2p; (d) P 2p spectra for the hybrid (1:1 ratio) thin film on metal; (e) Si 2p; (f) P 2p spectra of the LBL film with EGMP layer on top of MEMO layer.

carbon only bound to carbon and hydrogen (C–C, C–H), respectively, whereas the peak at 286.4 eV is attributed to the carbon making a single bond with oxygen (C–O). The peak at the higher binding energy (288.6 eV) is due to the carbon making one single bond and one double bond with oxygen (O=C–O) [26,27]. The O 1s peak is broad, indicating the different chemical states of oxygen. In order to understand the chemical state of oxygen present in the hybrid thin film, the O 1s peak was deconvoluted and fitted with three peaks centered at 531.5 eV, 532.5 eV and 533.2 eV. The peak at 531.5 eV is attributed to oxygen making a double bond with carbon and non-bridging oxygen in the phosphate group (P=O) [28]. The assignment of the peak at 532.5 eV is complex since binding energy of oxygen in C–O, P–O–C, P–O–Si and Si–O–Si appear in this region [29,30]. Hence, this peak is attributed to the combined effects of these oxygen chemical states. The third peak at higher binding energy at 533.2 eV is attributed to the symmetric oxygen bridging in P–O–P group [28]. The phosphorus peak appearing at 133.4 eV is attributed to the phosphate group. This peak is broad and deconvoluted into two peaks at 133.4 eV and 134.2 eV, which correspond to P–O–C/P–O–Si and P–O–P/P=O, respectively [30,31]. The Si 2p peak is centered at 102.6 eV with an additional component at 103.1 eV. The peak at 102.6 eV is assigned to Si–O–Si linkages in the polymeric network and the additional peak at 103.1 eV is ascribed to Si–O–P formation [31]. Thus, the XPS results confirm the FTIR results, which show the formation of Si–O–Si, P–O–Si and P–O–P linkages. Also, quantification of different chemical states is done and their comparison with theoretical value is given in Table 1. The experimental values are in good accordance with the theoretically predicted values.

In order to investigate, whether the interfacial region consists of preferentially one phase or mixed phase, thin film deposition was carried out using layer-by-layer (LBL) method. The same conditions used for the copolymer coating were used, except that MEMO was deposited and partially cured for 30 min at 120 °C prior to applying EGMP layer and

Table 1
Comparison of the surface chemical composition determined by XPS with the theoretical value

Element/atomic%	Binding energy (eV)/ assigned component	Chemical composition (%)	
		Experimental	Theoretical
C 1s/51.7	284/C–Si	7.7	7.6
	284.6/[C–(C, H)]	44.5	53.8
	286.4/C–O	32.7	23
	288.6/O–C=O	14.9	15.4
O 1s/39.8	531.5/C=O, P=O	30.1	30.1
	532.5/Si–O–Si, C–O, P–O–C, P–O–Si	57.1	53.8
	533.2/P–O–P	12.9	15.4
P 2p/3.8	133.4/P–O–C, P–O–Si	31	*
	134.2/P–O–P, P=O	69	*
Si 2p/4.7	102.6/Si–O–Si	66.4	*
	103.1/Si–O–P	33.6	*

*Denotes that these values could not be determined theoretically due to the inability of the theory to predict the amount of Si–O–P formation.

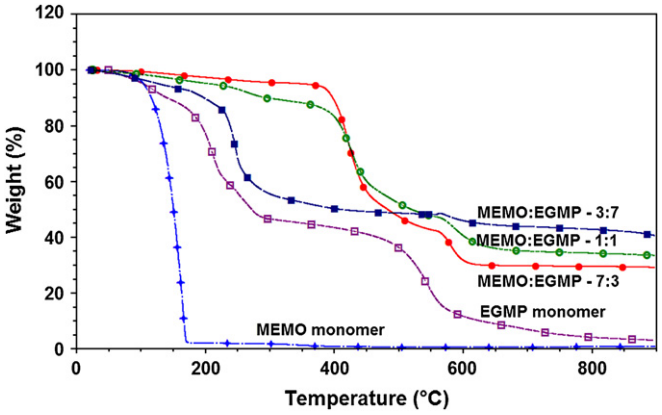

Fig. 5. Thermogravimetric curves of the hybrid thin film for three different compositions and the pure monomers.

vice-versa. It is interesting to note that when MEMO was first deposited followed by EGMP layer, almost negligible amount of silicon is observed with XPS [Fig. 4(e) and (f)]; due to preferential Si–O–Si network formation at the interface, whereas the layer-by-layer film with MEMO layer on top of the EGMP layer shows peaks corresponding to both phosphorus and silicon indicating interpenetrating polymer network (IPN) formation. This is in contrast with the results published elsewhere [1] indicating preferential migration of phosphate to the metal–film interface and siloxane to the film–air interface. This behavior can be attributed to the higher number of crosslinking sites in MEMO leading to a dense network during partial curing, thereby preventing the diffusion of EGMP through MEMO layer; whereas in case of MEMO on top of EGMP layer, MEMO diffuses through the EGMP layer and forms the interpenetrating network. This shows that the incorporation of MEMO in the polymer matrix increases the crosslinking density and also forms interpenetrating network.

To confirm the extent of interaction in the hybrid, an equilibrium swelling experiment was carried out with MEMO/EGMP – 1:1 hybrid. Disks were made from the hybrid and immersed in solvent (ethanol) used for the hybrid preparation at room temperature. It is interesting to note that the hybrid is not soluble in the solvent and shows equilibrium swelling of 2.6% over the period of 18 days. This confirms the presence of highly cross-linked structure of the hybrid as also confirmed by the FTIR.

3.2. Thermal analysis

The thermal degradation behavior of the prepared hybrid materials and the monomers were examined using TGA. The onset of degradation and the residue content at 900 °C were evaluated using the weight loss curves (Fig. 5). The maximum weight loss temperature, the amount of weight loss (both theoretically calculated and the experimental values) are given in Table 2. The theoretical weight percent of individual components were calculated by considering the repeating unit of the polymer chain and the stoichiometric feed ratio. The components corresponding to the degradation peaks are assigned based on the theoretical and experimental calculations of weight percentage of the individual components. The weight loss of the EGMP monomer below 140 °C can be attributed to the condensation of P–OH groups to form P–O–P linkages. The degradation of the EGMP monomer occurs in three main stages. The first major peak occurs in the temperature range of 190–221 °C and is assigned to the degradation of the P–O–C bond [32,33]. This is immediately followed by the degradation of the alkyl group [33] with the maximum weight loss (T_{MAX}) occurring at 259 °C. The third major weight loss occurs in the temperature range of 450–590 °C, due to decomposition of the methacrylate component. On the other hand, the complete evaporation of the MEMO monomer occurs before 175 °C. The onset of degradation of the hybrid material prepared at MEMO/EGMP – 3:7 ratio occurs at 178 °C due to the relative ease of degradation of the phosphate component. The initial decomposition of the phosphate group is followed by partial thermal pyrolysis of the alkyl chain and the methacrylate group with the maximum weight loss occurring at 246 °C. No further degradation of this hybrid is observed at higher temperatures. In the case of the hybrid with MEMO/EGMP – 1:1 ratio, the onset of degradation is shifted to higher temperature at 240 °C and the decomposition of the alkyl and methacrylate group occurs at higher temperature. The T_{MAX} corresponding to the degradation of alkyl and methacrylate groups occurs at 427 °C. The hybrid material prepared at MEMO/EGMP – 7:3 ratio shows higher thermal stability and the onset of degradation occurs at 333 °C followed by decomposition of the alkyl group and the methacrylate group. These results indicate that the thermal stability of the hybrid material increases with increase in the amount of MEMO. This can be attributed to increase in silica network with increase of MEMO content.

However, the amount of residue remained at 900 °C increases with increase in the phosphate content in the hybrid. The residue yield at 900 °C is estimated from Fig. 5 as 29.2%, 33.5% and 40.8% for 7:3, 1:1 and 3:7 MEMO/

Table 2
Thermal degradation of sol–gel derived hybrids and the monomers[a]

Molar ratio (MEMO/EGMP)	T_{onset} (°C)	T_{MAX1} (°C)	Weight loss (%)	T_{MAX2} (°C)	Weight loss (%)	T_{MAX3} (°C)	Weight loss (%)	Residue (%)
MEMO monomer	134	164	–	–	–	–	–	0.7
7:3	333	397	8.4 (8.7)	428.0	44.5 (41.1)	557.0	13.2 (14.2)	29.2 (34.8)
1:1	240	264	12.1 (14.4)	427.0	37.9 (41.1)	587.0	12.4 (10.1)	33.5 (33.3)
3:7	178	192	9.8 (20.2)	246.0	37.7 (41.1)	–	–	40.8 (31.8)
EGMP Monomer	92	210	29.8 (30.1)	259.0	13.6 (13.4)	544.0	36.8 (37.1)	3.1

[a] Theoretical weight loss percentage and theoretical residue percentage are given in the parentheses.

EGMP ratios, respectively. Their corresponding theoretical values are 34.8%, 33.3% and 31.8%, respectively. Based on theoretical and experimental residue results, the percent yield of the condensation reactions of inorganic components are found to be 84% and 100% for the 7:3 and 1:1 MEMO/EGMP ratios, respectively. In case of MEMO/EGMP – 3:7 sample, experimental residue content is much higher than theoretically predicted values. Such characteristics of the hybrid can be attributed to relative ease of degradation of the phosphate containing segment which degrades at relatively lower temperature and leaves some volatile material which catalyzes degradation of alkyl chain and forms a complex with carbon compounds. It leads to a phosphorus rich insulating layer [1,34] which thermally insulates the hybrid and prevents diffusion of combustible gases through organic layer. This reduces further degradation of the hybrid and hence an increase in residue is observed.

The glass transition (T_g) temperature of the thin film, a critical parameter which governs the barrier properties and establishes maximum service temperature of the thin film, has been determined from differential scanning calorimetry. The second heating cycle of the cured hybrid material for three different molar ratios is given in Fig. 6. The T_g of the hybrid material is found at 93 °C and it does not change with change in composition. Although, the inclusion of flexible –P–O– group in the polymer chain by incorporating phosphate group is known to lower the T_g [35], no such effect could be observed with the prepared hybrid. This could be explained by the presence of extensive crosslinking, which limits segmental mobility of the chains [34].

3.3. Micro-thermal analysis

The above thermal analysis represents average properties of the sample over the sample area under investigation. Further understanding on spatial distribution of individual phases of the samples with such complex structure needs to be established. Also, for thin film applications, morphology and surface coverage of the film on the substrate play vital role in their performance. Hence, micro-thermal analysis was carried out on coated samples to establish these parameters. The thermal conductivity image of the hybrid thin film (MEMO/EGMP – 1:1) on mild steel substrate is given in Fig. 7. There is no contrast in the thermal conductivity image of the thin film throughout the sample surface, which indicates that the thin film is uniform, homogenous and defect-free without any phase separation. Fig. 8 depicts the high magnification 3D topographic images of the hybrid thin films obtained from three different compositions of MEMO and EGMP. The surface roughness values were calculated from the topographic images and the root mean square (RMS) roughness values of 3:7, 1:1, 7:3 (MEMO/EGMP) samples are 0.25 nm, 0.42 nm and 0.56 nm, respectively. This shows that the surface becomes rougher with increasing MEMO content in the hybrid thin film, which is attributed to the formation of silicate network. Three random positions on the coated mild steel sample (MEMO/EGMP – 1:1) were selected for LTA and the probe was positioned at selected positions and the temperature ramp was applied. Fig. 9 shows the LTA plots of probe deflection as a function of applied temperature for each random location. Softening of the thin film occurs at around 100 °C. The T_g of the hybrid material obtained from

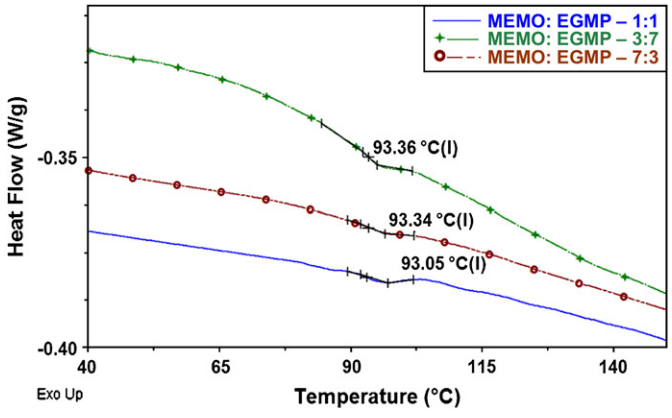

Fig. 6. DSC curves of hybrid thin films with MEMO/EGMP at 7:3, 1:1 and 3:7 ratios.

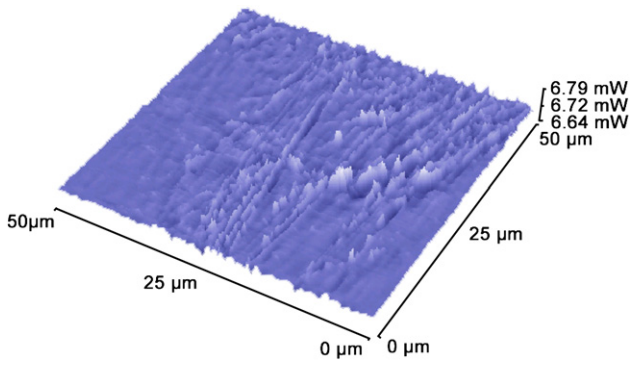

Fig. 7. Thermal conductivity image of the MEMO/EGMP – 1:1 hybrid thin film.

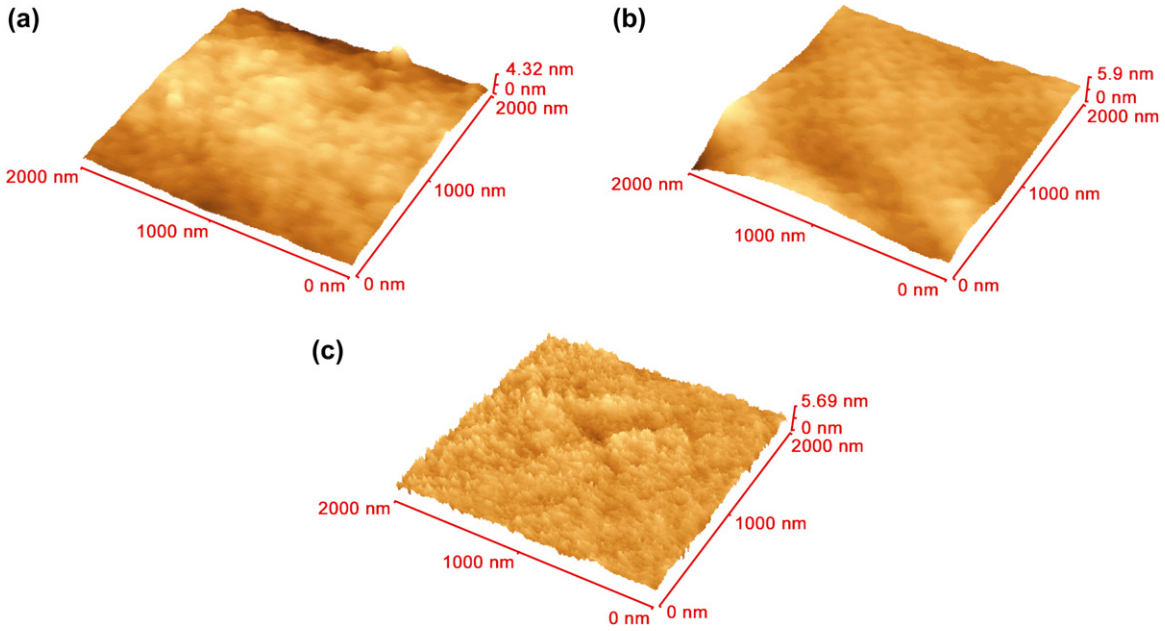

Fig. 8. Magnified topographic images of the thermally cured hybrid thin film (a) MEMO/EGMP – 3:7; (b) MEMO/EGMP – 1:1 and (c) MEMO/ EGMP – 7:3.

DSC is at 93 °C. This difference is attributed to the higher heating rate used in μTA. In addition, all the three plots obtained from three random locations are identical which illustrates the uniform nature of the thin film throughout the surface.

3.4. Mechanical properties

The mechanical properties of the thin films such as modulus and hardness were determined using nanoindentation as they could greatly influence the thin film coating performance. The elastic moduli and hardness values of the thin films were determined from the load–displacement curves obtained using nanoindentation experiments. Fig. 10 shows indentation responses for three different compositions with a 30 s dwell time at 0.2 mN load prior to unloading. No time dependent increase in the indenter penetration depth was observed for any of the hybrid film during holding period at a maximum load. The calculated hardness results follow the order for 3:7 < 1:1 < 7:3 MEMO/EGMP ratios with values of 0.47 ± 0.017 GPa, 0.48 ± 0.017 GPa and 0.54 ± 0.019 GPa, respectively. The modulus values range from 6.57 GPa to 11.07 GPa (with the experimental error of ±3.6%) and the highest value is obtained with 7:3 ratio, where maximum Si–O–Si network formation occurs. Thus, by increasing the hardness/modulus values, scratch resistance of the thin film can be strongly influenced. The hardness and modulus values obtained are intermediate between the values of methacrylate and the inorganic component, and similar results [36,37] have been reported for sol–gel derived hybrid thin films previously. Further evaluations of electrochemical properties of these hybrid thin films are currently underway and will be reported in our future publication.

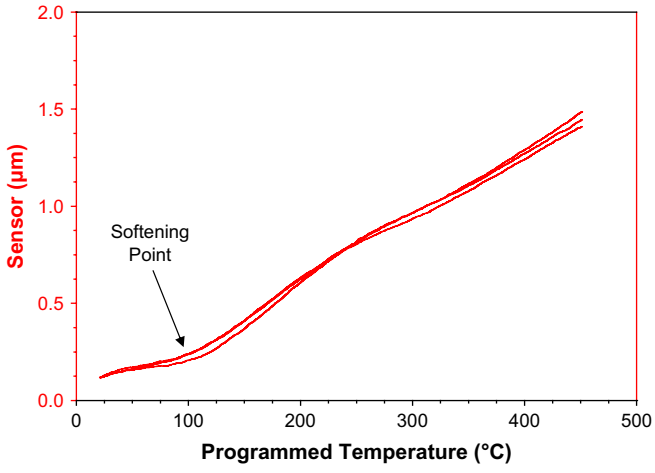

Fig. 9. LTA plots of the probe deflection with temperature at three different locations of MEMO/EGMP – 1:1 hybrid thin film.

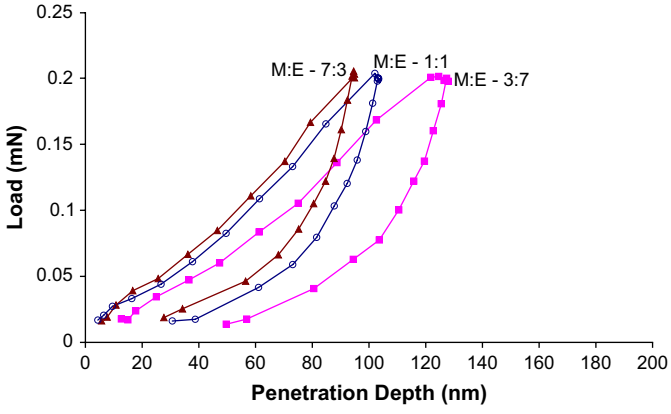

Fig. 10. Nanoindentation loading–hold–unloading curves of MEMO/EGMP hybrid thin film on mild steel substrates prepared at 3:7, 1:1 and 7:3 ratios.

4. Conclusions

In summary, we have demonstrated that a highly cross-linked dense hybrid material with phospho-silicate groups can be synthesized via a combination of sol–gel reaction and free radical polymerization. PA-FTIR and XPS results demonstrate the formation of highly cross-linked hybrid material through the formation of Si–O–Si, Si–O–P and P–O–P linkages and organic network through the polymerization of the methacrylate group. The cured hybrid material forms a highly networked, dense, uniform, homogenous and defect-free thin film on mild steel substrates, which makes this hybrid thin film ideal for protective application. The presence of phosphate functionality leads to strong interfacial interaction between the thin film and the substrate, whereas the silicate group enhances the thermal stability of the thin film. Amongst all, the hybrid containing 70 mol% MEMO shows the best performance for thin film applications.

Acknowledgements

The authors gratefully acknowledge the financial support of the Australian Research Council's Special Research Centre for carrying out this work.

References

[1] Mequanint K, Sanderson R, Pasch H. Polym Degrad Stab 2002;77:121–8.
[2] Rixens B, Severac R, Boutevin B, Lacroix-Desmazes P. J Polym Sci Part A Polym Chem 2006;44:13–24.
[3] Wang YC, Shen SY, Wu QP, Chen DP, Wang J, Steinhoff G, et al. Macromolecules 2006;39:8992–8.
[4] Suzuki S, Whittaker MR, Grondahl L, Monteiro M, Wentrup-Byrne E. Biomacromolecules 2006;7:3178–87.
[5] Sanchez C, Julian B, Belleville P, Popall M. J Mater Chem 2005;15:3559–92.
[6] Oaten M, Choudhury NR. Macromolecules 2005;38:6392–401.
[7] Schottner G. Chem Mater 2001;13:3422–35.
[8] Kickelbick G. Prog Polym Sci 2003;28:83–114.
[9] Wen J, Wilkes GL. Chem Mater 1996;8:1667–81.
[10] Brinker CJ, Scherer GW. Sol–gel science: the physics and chemistry of sol–gel processing. San Diego, CA: Academic Press; 1990.
[11] Saegusa T. Pure Appl Chem 1995;67:1965–70.
[12] Gao Y, Choudhury NR, Dutta N, Matisons J, Reading M, Delmotte L. Chem Mater 2001;13:3644–52.
[13] Medda SK, Kundu D, De G. J Non-Cryst Solids 2003;318:149–56.
[14] Wei Y, Jin D, Brennan DJ, Rivera DN, Zhuang Q, DiNardo NJ, et al. Chem Mater 1998;10:769–72.
[15] Soloukhin VA, Posthumus W, Brokken-Zijp JCM, Loos J, With GD. Polymer 2002;43:6169–81.
[16] Talbot D, Talbot J. Corrosion science and technology. CRC Press; 1998.
[17] Mequanint K, Sanderson R, Pasch H. J Appl Polym Sci 2003;88:900–7.
[18] Miller JB, Ko EI. Catal Today 1997;35:269–92.
[19] McClelland JF, Jones RW, Bajic SJ. FT-IR photoacoustic spectroscopy: handbook of vibrational spectroscopy. John Wiley & Sons; 2002.
[20] Dutta NK, Tran ND, Choudhury NR. J Polym Sci Part B Polym Phys 2005;43:1392–400.
[21] Ding J, Shi W. Polym Degrad Stab 2004;84:159–65.
[22] Liang H, Shi W. Polym Degrad Stab 2004;84:525–32.
[23] Xu P, Wang H, Tong R, lv R, Shen Y, Du Q, et al. Polym Degrad Stab 2006;91:1522–9.
[24] Ilieva D, Kovacheva D, Petkov C, Bogachev G. J Raman Spectrosc 2001;32:893–9.
[25] Yuan W, Ooij WJV. J Colloid Interf Sci 1997;185:197–209.
[26] Clark DT, Dilks A. J Polym Sci Part A Polym Chem 1979;17:957–76.
[27] Laoharojanaphand P, Lin TJ, Stoffer JO. J Appl Polym Sci 1990;40:369–84.
[28] Shih PY, Yung SW, Chin TS. J Non-Cryst Solids 1999;244:211–22.
[29] Li YS, Tran T, Xu Y, Vecchio NE. Spectrochim Acta A 2006;65:779–86.
[30] Chen X, Hu Y, Jiao C, Song L. Polym Degrad Stab 2007;92:1141–50.
[31] Massiot P, Centeno MA, Carrizosa I, Odriozola JA. J Non-Cryst Solids 2001;292:158–66.
[32] Lin CH, Wang CS. Polymer 2001;42:1869–78.
[33] Zhu S, Shi W. Polym Degrad Stab 2003;80:217–22.
[34] Wang Q, Shi W. Polym Degrad Stab 2006;91:1289–94.
[35] Jeng RJ, Wang JR, Lin JJ, Liu YL, Chiu YS, Su WC. J Appl Polym Sci 2001;82:3526–38.
[36] Atanacio JA, Latella BA, Barbe CJ, Swain MV. Surf Coat Tech 2005;192:354–64.
[37] Amerio E, Sangermano M, Malucelli G, Priola A, Voit B. Polymer 2005;46:11241–6.